BIOCHEMISTRY
including biophysical chemistry & molecular biology

Article

pubs.acs.org/biochemistry

Structural Basis for Nucleotide Binding and Reaction Catalysis in Mevalonate Diphosphate Decarboxylase

Michael L. Barta,[†,§] William J. McWhorter,[†] Henry M. Miziorko,*[,‡] and Brian V. Geisbrecht*[,†]

[†]Division of Cell Biology and Biophysics and [‡]Division of Molecular Biology and Biochemistry, School of Biological Sciences, University of Missouri—Kansas City, Kansas City, Missouri 64110, United States

Supporting Information

ABSTRACT: Mevalonate diphosphate decarboxylase (MDD) catalyzes the final step of the mevalonate pathway, the Mg^{2+}-ATP dependent decarboxylation of mevalonate 5-diphosphate (MVAPP), producing isopentenyl diphosphate (IPP). Synthesis of IPP, an isoprenoid precursor molecule that is a critical intermediate in peptidoglycan and polyisoprenoid biosynthesis, is essential in Gram-positive bacteria (e.g., *Staphylococcus*, *Streptococcus*, and *Enterococcus* spp.), and thus the enzymes of the mevalonate pathway are ideal antimicrobial targets. MDD belongs to the GHMP superfamily of metabolite kinases that have been extensively studied for the past 50 years, yet the crystallization of GHMP kinase ternary complexes has proven to be difficult. To further our understanding of the catalytic mechanism of GHMP kinases with the purpose of developing broad spectrum antimicrobial agents that target the substrate and nucleotide binding sites, we report the crystal structures of wild-type and mutant (S192A and D283A) ternary complexes of *Staphylococcus epidermidis* MDD. Comparison of apo, MVAPP-bound, and ternary complex wild-type MDD provides structural information about the mode of substrate binding and the catalytic mechanism. Structural characterization of ternary complexes of catalytically deficient MDD S192A and D283A (k_{cat} decreased 10^3- and 10^5-fold, respectively) provides insight into MDD function. The carboxylate side chain of invariant Asp^{283} functions as a catalytic base and is essential for the proper orientation of the MVAPP C3-hydroxyl group within the active site funnel. Several MDD amino acids within the conserved phosphate binding loop ("P-loop") provide key interactions, stabilizing the nucleotide triphosphoryl moiety. The crystal structures presented here provide a useful foundation for structure-based drug design.

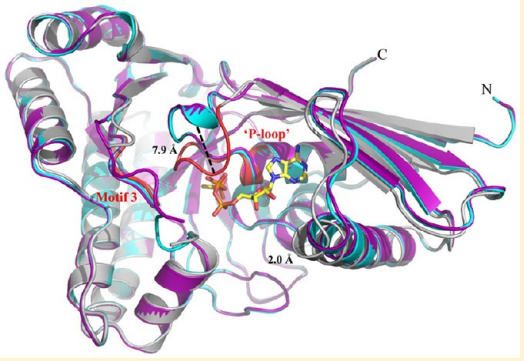

Synthesis of isopentenyl 5-diphosphate (IPP) is critical in eubacteria, where it serves as an essential intermediate in the synthesis of diverse polyisoprenoid compounds. Whereas Gram-negative bacteria utilize the methylerythritol phosphate pathway for the creation of IPP,[1] certain species of pathogenic Gram-positive organisms (such as *Staphylococcus aureus* and *Staphylococcus epidermidis*) utilize the mevalonate pathway.[2] In total, three molecules of acetyl-CoA are used to produce one molecule of IPP via the mevalonate pathway through six enzymatic steps. Within this sequence, there are three consecutive ATP-dependent reactions needed to produce IPP from mevalonic acid in a manner that is essential for bacterial viability.[2] The last of these reactions is catalyzed by the enzyme mevalonate diphosphate decarboxylase (MDD). MDD (EC 4.1.1.33) catalyzes the divalent cation-dependent,[3] irreversible decarboxylation of mevalonate 5-diphosphate (MVAPP) into IPP, along with the concurrent hydrolysis of ATP to ADP and formation of CO_2 and inorganic phosphate.[4] The reaction proceeds as follows:

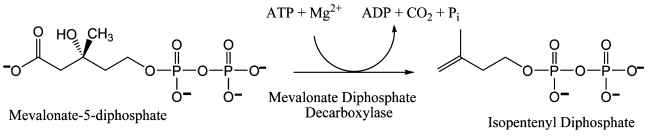

The mevalonate pathway is operative in higher-order eukaryotes, plants, some protists, and many Gram-positive prokaryotes, so the extensive characterization of MDD from yeast,[4,5] avian,[6] and mammalian sources[6−8] has elucidated many details of the MDD mechanism (the numbering of all residues herein reflects their position in the *S. epidermidis* MDD sequence). Deprotonation of the acceptor MVAPP C3-hydroxyl occurs via the general base Asp^{283}, which leads to a phosphorylation to form the putative metastable 3-phospho-MVAPP adduct.[9] Creation of a carbocation intermediate at the C3 position results from the departure of the newly transferred phosphoryl. Decarboxylation proceeds after the formation of this intermediate via the interaction of Arg^{144} with the C1-carboxylate of MVAPP and thereby yields the product, IPP. Mutagenesis studies of both of these side chains revealed an upward of 10^3-fold decrease in catalytic activity, which confirmed the function of these residues' side chains in catalysis.[5,10]

Received: May 7, 2012
Revised: June 25, 2012
Published: June 26, 2012

Table 1. Diffraction Data Collection and Structure Refinement Statistics

	S192A MDD	S192A MDD	S192A MDD	MDD	D283A MDD	MDD	D283A MDD
			Diffraction Data[a]				
ligands		DPGP	FMVAPP, ATPγS	FMVAPP, ATPγS	MVAPP, ATPγS	MVAPP	DPGP
beamline	APS 22-ID	APS 22-ID	APS 22-ID	APS 22-ID	APS 22-ID	APS 22-BM	APS 22-BM
space group	$C222_1$	$C222_1$	$C222_1$	$C2$	$P2_12_12_1$	$C222_1$	$C222_1$
no. of molecules in asymmetric unit	2	2	2	2	8	2	2
unit cell parameters							
a (Å)	82.922	82.678	82.732	102.251	96.459	82.592	82.966
b (Å)	102.273	101.733	103.14	82.46	99.445	101.32	102.05
c (Å)	155.942	155.498	156.749	93.649	314.418	154.932	155.143
β (deg)				122.34			
wavelength (Å)	1.0000	1.0000	1.0000	1.0000	1.0000	1.0000	1.0000
resolution (Å)	50.0−1.95	50.0−2.15	50.0−1.90	50.0−2.19	50.0−2.60	50.0−2.20	50.0−2.10
completeness (%)	100.0 (100.0)	91.7 (82.0)	99.7 (99.6)	99.9 (99.4)	98.2 (99.9)	99.8 (99.1)	95.0 (88.1)
total no. of reflections	355071	195781	539192	183389	699223	306240	232548
no. of unique reflections	48719	33395	52862	33632	91579	33287	36836
redundancy (x-fold)	7.3	5.9	10.2	5.5	7.6	9.2	6.3
R_{merge} (%)[b]	8.3 (38.2)	7.6 (32.0)	8.0 (58.4)	7.5 (49.7)	20.3 (59.2)	11.7 (55.7)	9.3 (53.8)
$\langle I\rangle/\langle\sigma I\rangle$	19.3 (5.83)	15.7 (5.29)	20.5 (3.2)	19.7 (3.31)	7.57 (3.75)	19.8 (3.04)	19.3 (3.58)
PDB entry	4DPX	4DPY	4DPU	4DPT	4DPW	4DU7	4DU8
			Refinement				
R_{work}/R_{free}[c]	16.24/20.01	16.75/22.62	17.91/22.37	18.62/24.07	19.87/25.08	19.15/23.88	18.63/23.87
rmsd							
bond lengths (Å)	0.007	0.008	0.007	0.010	0.009	0.007	0.007
bond angles (deg)	1.005	1.017	1.058	1.192	1.121	0.971	1.001
Ramachandran							
favored (%)	98.6	98.0	98.5	96.5	97.7	98.6	98.0
allowed (%)	1.4	2.0	1.4	3.3	2.3	1.4	2.0
outliers (%)	0.0	0.0	0.2	0.2	0.0	0.0	0.0
no. of atoms							
protein	5102	5102	5125	5017	20,386	5055	5074
solvent	587	399	488	256	266	275	293
ligand	N/A[d]	40	100	50	392	36	40
B factor (Å^2)							
protein	23.2	26.5	27.9	37.7	50.9	35.0	27.7
solvent	30.6	29.3	31.8	37.6	51.0	34.6	28.9
ligand	N/A[d]	23.5	27.9	55.3	45.7	30.9	29.3
density gallery[e]		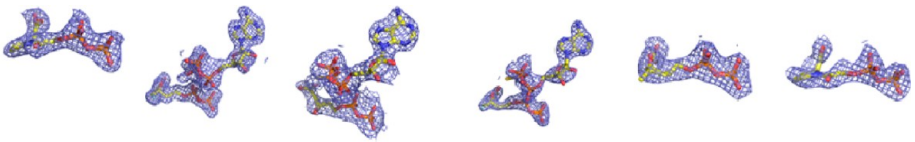					

[a]Numbers in parentheses are for the highest-resolution shell. [b]$R_{merge} = \sum_h\sum_i|I_i(h) - \langle I(h)\rangle|/\sum_h\sum_i I_i(h)$, where $I_i(h)$ is the ith measurement of reflection h and $\langle I(h)\rangle$ is a weighted mean of all measurements of h. [c]$R = \sum_h|F_{obs}(h) - F_{calc}(h)|/\sum_h|F_{obs}|$. R_{cryst} and R_{free} were calculated from the working and test reflection sets, respectively. The test set constituted 5% of the total reflections not used in refinement. [d]Not available. [e]The $2F_o - F_c$ electron density maps (blue mesh contoured at 1.0σ) of modeled ligands.

MDD is a member of the GHMP kinase (galactokinase, homoserine kinase, mevalonate kinase, phosphomevalonate kinase) family.[11] These enzymes are characterized by a cone-shaped fold with a deep active site cleft that houses the previously mentioned catalytic Asp and Arg residues, while the β-grasp-like N-terminal region packs against the C-terminal five-α-helix bundle.[12] Although previous work resulted in the determination of a number of different MDD crystal structures,[10−12] none of these studies succeeded in crystallizing the enzyme in a metabolite or ligand-bound form. More recently, however, our group reported the high-resolution cocrystal structures of *S. epidermidis* MDD bound to the inhibitory substrate analogues diphosphoglycolylproline (DPGP) and 6-fluoromevalonate diphosphate (FMVAPP).[13] Both FMVAPP and DPGP are competitive inhibitors, though their K_i values (50 nM and 4.3 μM, respectively) differ considerably. Comparison of their respective crystal structures when bound to MDD provided a physical explanation for this difference.[13] Inspection of these structures also identified the side chain of invariant Ser[192] as making potential contributions to catalysis. Indeed, loss of Ser[192] resulted in a nearly 10^3-fold decrease in k_{cat} compared to that of wild-type MDD.

Unfortunately, one limitation of these recent structures was that they lacked a bound nucleotide within the MDD active site. This restricted any mechanistic conclusions about those features that concerned the phosphoryl acceptor, MVAPP.

dx.doi.org/10.1021/bi300591x | *Biochemistry* 2012, 51, 5611−5621

Thus, to characterize the MDD structure, active site, and catalytic mechanism more completely, we report here a series of seven additional high-resolution X-ray cocrystal structures of *S. epidermidis* MDD bound to both inhibitory substrate analogues and the nucleotide analogue ATPγS. Included in this cohort are ternary complexes of two previously characterized catalytically deficient MDD mutants, S192A[13] and D283A,[5] bound to inhibitory substrate analogues as well as the nucleotide analogue ATPγS. Analysis of these mutant MDD ternary complexes, along with that of wild-type MDD bound to FMVAPP and ATPγS, has provided significant insight into the conformational changes that occur upon nucleotide binding and thereby significantly augments our collection of structural "snapshots" of the reaction cycle.

With antibiotic resistant strains of Gram-positive bacterial organisms becoming an increasingly serious healthcare issue,[14,15] focusing on the identification of novel classes of antimicrobial drugs is now of paramount importance. The apparently essential nature of the mevalonate pathway ATP-dependent kinases for bacterial cell viability strongly suggests that these enzymes are excellent targets for antimicrobial compounds.[2] In this regard, it is worth noting that recent investigation of small molecule inhibitors that selectively target the nucleotide binding region within ATP-dependent enzymes has met with great success.[16] Thus, we believe that development of selective inhibitors that target the substrate and nucleotide binding regions of bacterial MDDs will be greatly aided by the structure–function studies presented and discussed here.

EXPERIMENTAL PROCEDURES

Materials. Unless specified, all chemical and biological products used in these studies were reagent grade materials purchased from Fisher Scientific or Sigma-Aldrich.

Substrates and Analogues. The synthesis of mevalonate 5-diphosphate (MVAPP) has been previously reported[17] and briefly summarized elsewhere.[13] 6-Fluoromevalonate diphosphate (FMVAPP) was prepared via the method described by Voynova et al.[10] and also described previously.[13] The competitive inhibitor diphosphoglycolylproline (DPGP) was synthesized by the strategy of Vlattas et al.[18] using the methodology described by Krepkiy and Miziorko.[9] ATPγS was purchased from Calbiochem.

Cloning, Overexpression, and Purification of MDD. Expression and purification of wild-type and S192A *S. epidermidis* MDD were described previously.[13] An analogous expression vector for the $Asp^{283} \rightarrow Ala$ mutant was constructed using standard molecular biology techniques.[19] Expression and purification of this mutant enzyme were performed in a manner equivalent to that of the wild-type protein.

Crystallization. Crystallization of *S. epidermidis* MDD was described previously.[13] Briefly, 1 μL of protein solution [5 mg/mL in 10 mM Tris-HCl (pH 7.5) and 50 mM NaCl] was mixed with 1 μL of reservoir solution containing 0.25 M sodium formate and 16% (w/v) PEG 3350 that had been previously diluted in an equal volume of ddH_2O and equilibrated over 500 μL of reservoir solution. Crystals of apo-S192A MDD were obtained in an analogous manner. Cocrystallization of MDD (wild-type or mutant) with a molar excess (~0.5 mM) of ligands (50 mM $MgCl_2$ for ternary cocrystallization) was achieved in a similar fashion. Cocrystallization through the substitution of magnesium formate in place of sodium formate for all ternary experiments was also performed in an attempt to obtain Mg^{2+}-bound MDD. All crystals were flash-cooled in a cryoprotectant solution consisting of reservoir buffer with an additional 15% (v/v) glycerol. Ternary complex cocrystals were flash-cooled in a cryoprotectant containing additional 50 mM $MgCl_2$.

Diffraction Data Collection, Structure Determination, Refinement, and Analysis. Monochromatic X-ray diffraction data were collected from single crystals at 100 K using beamlines 22-ID and 22-BM of the Advanced Photon Source, Argonne National Laboratory (Table 1). Following data collection, individual reflections were indexed, integrated, merged, and scaled using HKL2000.[20] Initial phase information was obtained for all MDD structures by maximum-likelihood molecular replacement using PHASER.[21] Chain A of Protein Data Bank (PDB) entry 3QT5 (*S. epidermidis* MDD) was used as a search model. The single most highly scored solution for each molecular replacement search contained two copies of MDD in the asymmetric unit for crystals of space group $C222_1$ or $C2$, while crystals within space group $P2_12_12_1$ contained eight copies of MDD within the asymmetric unit.

Structure refinement was conducted using the protocols implemented in *phenix.refine*.[22] One round of individual coordinate and isotropic atomic displacement factor refinement was conducted, and the refined model was used to calculate both $2F_o - F_c$ and $F_o - F_c$ difference maps. These maps were used to iteratively improve the model by manual building in Coot,[23,24] followed by additional coordinate and atomic displacement factor refinement. Ordered solvent molecules were added to all structures according to the default criteria of *phenix.refine* and inspected manually using Coot prior to the completion of the model. Additional information and refinement statistics for all seven structures are listed in Table 1.

Regions of poor electron density prevented the complete modeling of each polypeptide in the asymmetric unit within several of the structures described here. Typically, these regions of low map quality were between residues 185 and 191. Further details regarding the residues that could not be modeled accurately may be found in the corresponding PDB files.

Ligand Fitting. Models for each ligand were generated using the PRODRG server,[25] and restraint files were generated using *phenix.elbow*.[22] Inspection of the initial $F_o - F_c$ maps described above revealed unmodeled contiguous density that corresponded to ordered ligands in the active site of all copies of MDD found within the asymmetric unit, with a single exception. Only a single active site within the cocrystal structure of wild-type MDD bound to FMVAPP and ATPγS was found to be occupied; thus, the second copy of MDD within the asymmetric unit was modeled in the apo conformation. Subsequently, *phenix.ligandfit* [22] was subsequently used to fit and model an inhibitor, substrate, and/or nucleotide molecule in each active site. Refinement of complexed MDD structures was conducted as described above, with the exception that constrained group occupancy refinement was used to estimate the fraction of ligand bound at each site independently (Table 1 of the Supporting Information).

Miscellaneous. Multiple-sequence alignments were conducted using CLUSTALW[26] and aligned with secondary structure elements using ESPRIPT.[27] The following MDD sequences were used in alignments (GenBank entries in parentheses): *S. epidermidis* (27467280), *S. aureus* (14246359), *Legionella pneumophila* subsp. *pneumophila* (52842257), *Streptococcus pyogenes* (5093120), *Homo sapiens*

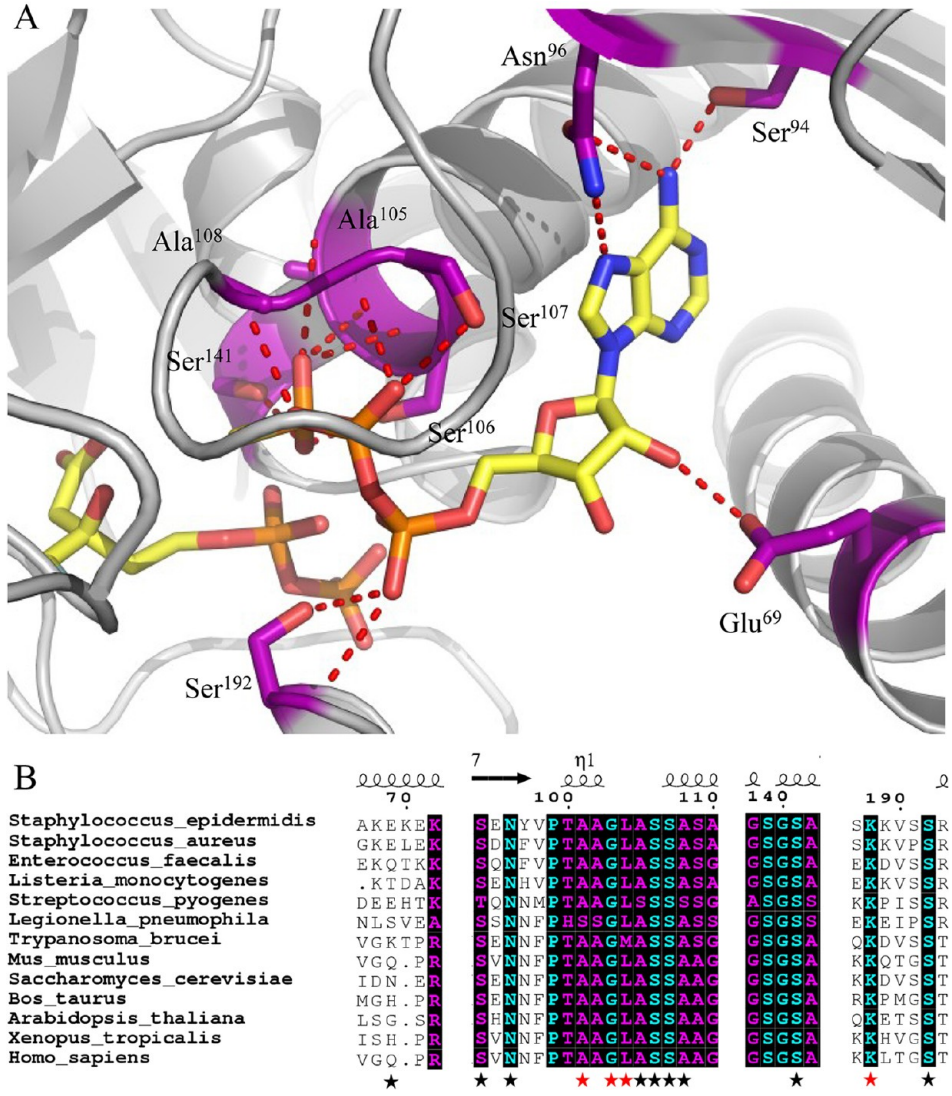

Figure 1. Cocrystal structure (2.19 Å) of MDD from *S. epidermidis* bound to inhibitor FMVAPP and nucleotide analogue ATPγS. (A) Cocrystal structure of *S. epidermidis* MDD in cartoon format (gray). Inhibitor FMVAPP and nucleotide analogue ATPγS are shown as balls and sticks (yellow). Active site side chains within interaction distance (2.5−3.4 Å) of ATPγS are shown as balls and sticks (purple) with red dashes. Hydrogen bonding distances can be found in Table 3 of the Supporting Information. (B) Limited structure-based sequence alignment of prokaryotic and eukaryotic MDD proteins colored according to residue conservation (cyan for absolute and purple for similar). Alignment was generated using ClustalW. Numbers above the sequences correspond to *S. epidermidis* MDD. Black stars below the sequences denote WT MDD amino acid side chains involved in ATPγS interaction, while red stars denote additional ATPγS interactions in the D283A mutant.

(4505289), *Saccharomyces cerevisiae* (1706682), *Trypanosoma brucei* (149241992), *Mus musculus* (13539580), *Listeria monocytogenes* (217965923), *Enterococcus faecalis* (315577315), *Xenopus* (*Silurana*) *tropicalis* (39645379), *Bos taurus* (115495513), and *Arabidopsis thaliana* (18410026). Three-dimensional structures were superimposed using the Local-Global Alignment method (LGA).[28] Representations of all structures were generated using PyMol.[29] The coordinates for ligand AMP-PNP were obtained from *Streptococcus pneumoniae* PDB entry 3GON.[30]

RESULTS

The Cocrystal Structure of a *S. epidermidis* MDD Ternary Complex Illustrates the Conserved Nature of the Nucleotide Binding Site. We undertook cocrystallization trials of the *S. epidermidis* enzyme in the presence of the competitive inhibitor FMVAPP and various nucleotide analogues (ATPγS, AMP-PCP, and AMP-PNP) to identify and investigate the ATP binding site of MDD. Large, birefringent crystals were obtained only with the combination of FMVAPP and ATPγS and diffracted synchrotron X-rays to 2.19 Å resolution (Table 1). Intriguingly, this crystal belonged to space group *C*2, while both apo and inhibitor-only bound *S. epidermidis* MDD crystals belonged to space group $C222_1$.[13] The structure of this crystal was determined by molecular replacement using a single copy of unliganded *S. epidermidis* MDD as a search model. Analysis of the highest-scoring solution revealed two copies of MDD within the *C*2 asymmetric unit, as was previously described for the MDD crystals in $C222_1$; however, the change to a lower-symmetry lattice indicated that the crystal packing interactions had been altered by the presence of the nucleotide analogue ATPγS. Following initial modeling of both MDD copies, analysis of the $F_o - F_c$ difference maps indeed revealed two regions of strong,

dx.doi.org/10.1021/bi300591x | *Biochemistry* 2012, 51, 5611−5621

contiguous density housed within a single MDD active site cleft (Figure 1A of the Supporting Information). A single copy of both FMVAPP and ATPγS was modeled within this active site and refined to final occupancy values of 78 and 79%. Overall, the final structure is in good agreement with the observed diffraction data, as judged by R_{work} and R_{free} values of 18.6 and 24.1%, respectively (Table 1 and Table 1 and Figure 2A of the Supporting Information).

Numerous amino acid backbone atoms and residue side chains (invariant across all species of MDD) are involved in the extensive interaction between MDD and ATPγS (Figure 1A,B). Conserved amino acids Ser^{94} and Asn^{96} contribute three side chain hydrogen bonding pairs to the nucleotide purine ring, while the only nonconserved side chain interaction between MDD and ATPγS is found between the side chain of Glu^{69} and the ribose 2′-hydroxyl of the nucleotide. We recently documented a catalytic role for Ser^{192} [13] by demonstrating that an S192A mutant of MDD undergoes a $>10^3$-fold diminution in catalytic activity (k_{cat}). Interestingly, this mutant did not affect the location or K_M of substrate binding (near wild-type values). The side chain and backbone nitrogen of Ser^{192} are within appropriate hydrogen bonding distances of the α-phosphoryl group of ATPγS (Table 2 of the Supporting Information), which suggests that the catalytic roles of this amino acid include positioning the nucleotide triphosphoryl moiety. The remainder of the MDD−ATPγS interaction sites are located on the opposite side of the active site cleft from Ser^{192} and fall primarily within the consensus GHMP kinase phosphate binding loop (residues P-X_{aaa}-GLASSAA).[31−33]

Despite the fact that 50 mM $MgCl_2$ was used in the buffer during ternary wild-type MDD crystallization trials, no interpretable electron density was observed to suggest a stably coordinated Mg^{2+} atom. Indeed, the distance between the C3-hydroxyl of FMVAPP and the γ-phosphoryl of ATPγS is nearly 5.5 Å. This relatively large distance may very well be due to the absence of a coordinated Mg^{2+} ion, which is expected to be required for detection of a catalytically productive conformation for this complex.

Conformational Changes within MDD upon Nucleotide Binding. Even in the crystalline state, wild-type enzymes are known to be quite catalytically efficient.[34] This typically precludes the simultaneous use of bona fide substrate (i.e., MVAPP) and nucleotide (i.e., ATP) compounds in cocrystallography studies. To circumvent this problem, our initial work described above employed both FMVAPP and ATPγS, which are inhibitory analogues of their MDD substrate and nucleotide targets, respectively. However, the use of these analogues may also have contributed to the excessive distance between the γ-phosphoryl of ATPγS and the C3-hydroxyl of FMVAPP. To discern whether binding of FMVAPP rather than MVAPP within the MDD active site resulted in any conformational changes, we obtained a cocrystal structure of the MVAPP-bound enzyme at 2.20 Å limiting resolution (Table 1). Nearly identical binding modes and active site contacts are observed in both MVAPP-bound (Figure 2A) and FMVAPP-bound[13] wild-type MDD. Additionally, superposition of the main chain atoms from both MDD cocrystal structures reveals that 322 of 324 MVAPP-bound Cα atoms align within a 5.0 Å distance with those of the FMVAPP-bound enzyme at an overall rmsd of 0.40 Å (Table 3 of the Supporting Information). Thus, the nearly indistinguishable active site and tertiary structures in both cocrystal structures strongly suggest that binding of neither the MVAPP substrate nor the FMVAPP inhibitor results in conformational differences within MDD.

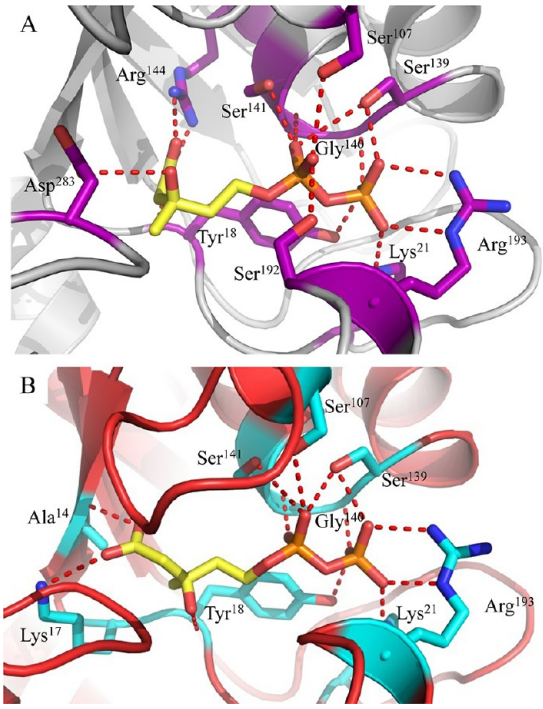

Figure 2. Cocrystal structures of WT and D283A MDD bound to the substrate MVAPP. (A) 2.20 Å cocrystal structure of *S. epidermidis* WT MDD in cartoon format (gray). Substrate MVAPP is shown as balls and sticks (yellow). Active site side chains within interaction distance of MVAPP are shown as balls and sticks (purple). (B) 2.10 Å cocrystal structure of *S. epidermidis* D283A MDD in cartoon format (red). Substrate MVAPP is shown as balls and sticks (yellow). Active site side chains within interaction distance of MVAPP are shown as balls and sticks (cyan). Hydrogen bonding distances can be found in Table 4 of the Supporting Information.

By contrast, structural superposition of apo MDD, MDD bound to MVAPP, and MDD bound to both FMVAPP and ATPγS reveals several conformational changes within MDD that arise only upon nucleotide binding (Figure 3). The conserved phosphate binding loop ("P-loop") clamps down around the triphosphoryl group of ATPγS and culminates in a movement that spans ∼7.9 Å as measured from the Cα atom of Ala^{110} within each enzyme. Similar conformational changes within the P-loop have been previously documented for other GHMP kinase family members upon nucleotide binding.[35,36] For example, within the ternary complex of homoserine kinase, the "upper lip" (residues 181−189) moves ∼3.5 Å to interact with the β-phosphoryl of ATP while Arg^{187} swings around 180° and entraps homoserine within the active site cleft.[37,38] Arg^{144} within *S. epidermidis* MDD has a similar effect and locks MVAPP into the active site funnel.[13] Separately, within the rat mevalonate kinase−ATP binary complex, the active site was deemed to be too large to snugly fit the mevalonic acid substrate; this prompted the authors to suggest that side chain reorientations and loop movements would likely need to occur in a ternary complex.[39] Indeed, an additional 2.0 Å movement within helix 1 (residues 69−83) further constricts the active site cleft upon formation of the MDD ternary complex presented here.

With these conformational changes now documented, superpositioning of the apo, MVAPP-bound, and ternary *S.*

dx.doi.org/10.1021/bi300591x | *Biochemistry* 2012, 51, 5611−5621

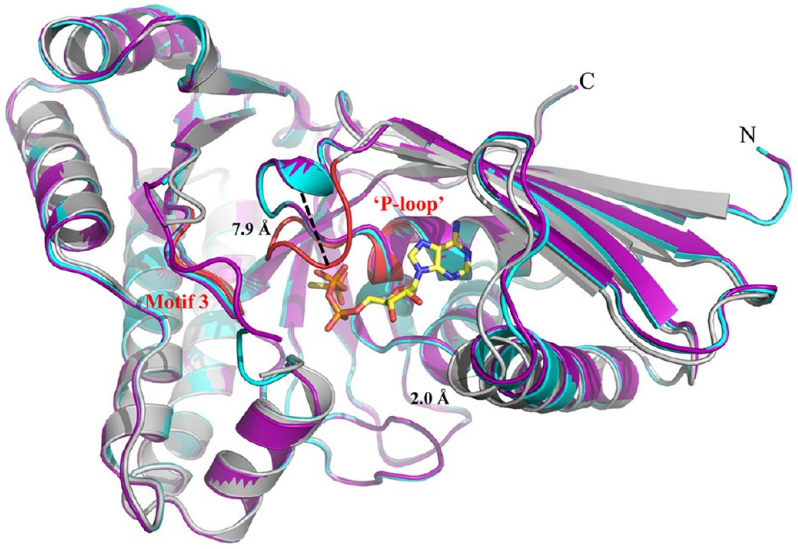

Figure 3. Structural alignment of WT MDD crystal structures. Cartoon ribbon diagram of the structural alignment of apo-MDD (purple), MDD bound to the substrate MVAPP (cyan), and MDD bound to the inhibitor FMVAPP and nucleotide analogue ATPγS (gray). Only ATPγS is shown for the sake of clarity as balls and sticks (yellow). Conserved GHMP kinase family motifs 2 (P-loop) and 3 are colored red within the ternary MDD cocrystal structure. A 7.9 Å shift within the P-loop, as measured from the Cα atom of Ala^{110} on both the apo-MDD and ternary MDD crystal structures, is highlighted for the sake of clarity. rmsd values for the structural alignment of all three structures can be found in Table 1 of the Supporting Information.

epidermidis MDD crystal structures can be used to provide informative visual cues about the sequential binding of the MVAPP acceptor and ATP donor substrates into the enzyme active site (Figure 4). First, the MVAPP substrate must first enter the unoccupied active site. MVAPP binds in the interior-most region of this funnel-shaped cavity, in the proximity of catalytic residues Arg^{144} and Asp^{283}.[13] No apparent structural changes are required to allow or result from acceptor binding. Next, the phosphoryl donor ATP binds at the active site periphery, atop the already positioned MVAPP. Upon assuming this ternary state, however, the MDD P-loop must clamp down upon the nucleotide triphosphoryl group. This rearrangement allows for the phosphoryl transfer and subsequent decarboxylation to proceed, at which time the structural changes can reverse to allow release of the product ADP and IPP.

Structural Basis for Catalytic Deficiencies in MDD Mutants. Previous structure–function studies of various MDDs have identified several residues that serve crucial roles in enzyme catalysis.[5,9,10,13] Among these, kinetic evaluations of mutants of two such residues (Ser^{192} and Asp^{283}) are especially intriguing. The S192A mutant exhibits an ∼1000-fold decrease in catalytic rate (k_{cat} = 0.0058 s^{-1}), despite its near wild-type K_M for MVAPP (5.0 μM) and its slightly decreased K_M for ATP (70 μM).[13] Curiously, however, the active site side chain interactions of the previously described S192A MDD–FMVAPP complex agree well with those obtained for the wild-type enzyme.[13] To characterize the S192A MDD mutant more fully, we obtained ternary cocrystals of FMVAPP and ATPγS bound to S192A MDD that diffracted X-rays to 1.90 Å resolution (Table 1). Interestingly, this cocrystal belongs to space group $C222_1$ and has unit cell dimensions that are nearly identical to those of either apo or FMVAPP-bound MDD.[13] Following structure solution and initial refinement, inspection of $F_o - F_c$ difference maps revealed regions of contiguous, well-defined electron density visible in both enzyme active sites (Figure 1B of the Supporting Information). This allowed modeling of both FMVAPP and ATPγS at high occupancy (>70%) prior to final refinement to R_{work} and R_{free} values of 17.9 and 22.4%, respectively. Several active site side chain and backbone interactions (Figure 5A) are present that compare favorably with those of the WT ternary complex. However, the absence of Ser^{192} appears to adversely affect the localization of the triphosphoryl group of ATPγS. Most significantly, the P-loop remains locked in the apo conformation, as superposition of this ternary structure with apo-S192A MDD shows that all 330 Cα atoms align within 5.0 Å with an rmsd of 0.49 Å (Table 3 of the Supporting Information). Thus, even though both substrate analogues are present, a lack of conformational change in the P-loop region accounts for the fact that these crystals maintain the same space group as both the apo and FMVAPP-bound forms.[13]

Studies of the catalytic base Asp^{283} revealed that a D283A mutant in *S. cerevisiae* MDD displays a 10^5-fold decrease in catalytic rate ($k_{cat} = 1.64 \times 10^{-5}$ s^{-1}) and a 3-fold inflation in the K_M for MVAPP (397 μM), but a K_M for ATP could not be directly determined because of the low activity of this mutant at subsaturating ATP levels, as well as a low intrinsic ATPase activity.[5] To structurally examine the ATP binding behavior of this mutant, we cocrystallized the D283A variant of *S. epidermidis* MDD as a ternary complex with MVAPP and ATPγS. These crystals diffracted X-rays to 2.60 Å limiting resolution, belonged to space group $P2_12_12_1$, and had vastly larger cell dimensions than any of those so far obtained for *S. epidermidis* MDD (Table 1). Following structure solution and initial refinement, contiguous regions of high-quality density were visible in each MDD active site within all eight copies in the asymmetric unit upon inspection of the $F_o - F_c$ difference maps (Figure 1C of the Supporting Information). This allowed modeling of both MVAPP and ATPγS at high occupancy (>88%) prior to final refinement to R_{work} and R_{free} values of 19.9 and 25.1%, respectively.

The D283A ternary complex active site reveals numerous additional MDD–ATPγS interactions (Figure 5B). In particular, several novel backbone atom interactions are present

dx.doi.org/10.1021/bi300591x | *Biochemistry* 2012, 51, 5611–5621

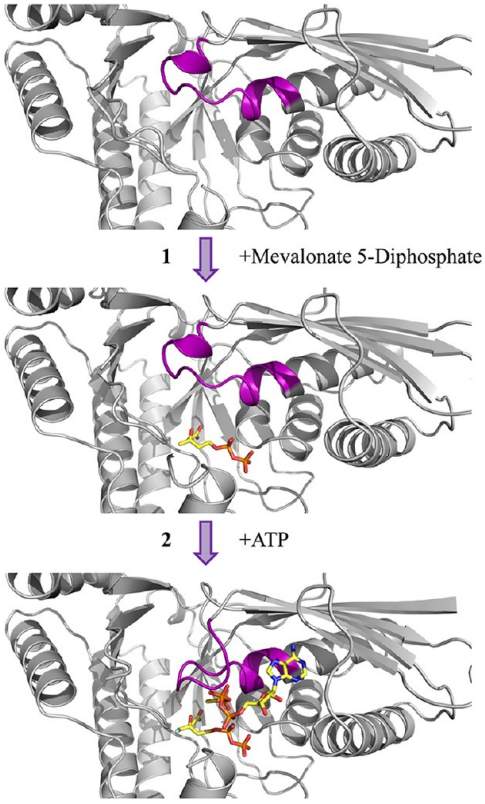

Figure 4. Sequential binding of substrate and nucleotide within the active site of MDD: (top) cartoon ribbon diagram of apo-MDD (gray), (middle) cartoon ribbon diagram of MDD (gray) in complex with the substrate MVAPP (balls and sticks, yellow), and (bottom) cartoon ribbon diagram of MDD (gray) in complex with the inhibitor FMVAPP and nucleotide analogue ATPγS (balls and sticks, yellow). In all three panels, the conserved P-loop sequence ($PTX_{aaa}GLASSAS$) is colored purple. The conformational change within the P-loop occurs after both substrate and nucleotide have bound to the enzyme active site.

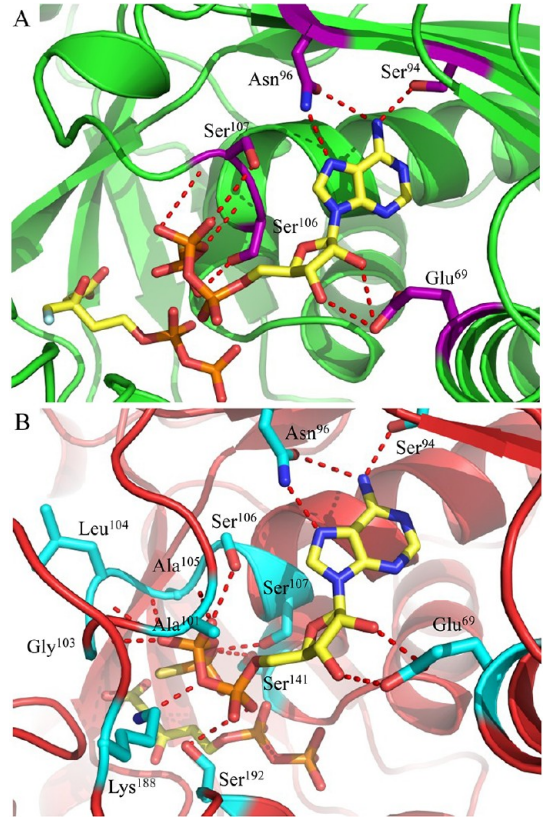

Figure 5. Active sites of ternary cocrystal structures from mutant forms of MDD. (A) 1.90 Å cocrystal structure of *S. epidermidis* S192A MDD in cartoon format (green). Inhibitor FMVAPP and nucleotide analogue ATPγS are shown as balls and sticks (yellow). Active site side chains within interaction distance of ATPγS are shown as balls and sticks (purple). (B) 2.60 Å cocrystal structure of *S. epidermidis* D283A MDD in cartoon format (red). Substrate MVAPP and nucleotide analogue ATPγS are shown as balls and sticks (yellow). Active site side chains within interaction distance of ATPγS are shown as balls and sticks (cyan). Hydrogen bonding distances can be found in Table 3 of the Supporting Information.

within the P-loop (Ala^{101}, Gly^{103}, and Leu^{104}), while the loop region connecting β-sheet 9 and helix 5 (residues 182−192) has swung into a position that allows conserved Lys^{188} to interact with the γ-phosphoryl group of ATPγS. Furthermore, the acceptor substrate binding site appears to be the same as that of the wild type within the D283A mutant, with the exception of a notable 120° rotation of the carboxylate and C3-hydroxyl groups of MVAPP (compare panels A and B of Figure 2). The absence of Asp^{283}, which has largely been confirmed as the general base responsible for deprotonation[5] and is believed to aid in the orientation of the MVAPP C3-hydroxyl,[9] provides a reasonable explanation for this misorientation.

Superposition of all three ternary MDD complexes sheds light on the structural alterations and mechanistic impact key mutations have on MDD catalysis (Figure 6A). Conformational changes within the P-loop appear very similar for both wild-type and D283A MDD, while the loop region in S192A appears unchanged. Indeed, both loops are repositioned by ∼8.1 Å (as measured from wild-type or D283A Ala^{101} Cα to S192A Ala^{101} Cα) to enclose the triphosphoryl moiety of ATPγS. Large-scale variances in the position of β-sheet 9 and the helix 5 connecting loop are also seen, as an ∼9.0 Å shift away from the active site (as measured from D283A Gln^{186} Cα to S192A Gln^{186} Cα) is observed for the S192A complex relative to the D283A complex. Analysis of the active site funnel dimensions (Figure 6B−D) further corroborates the functional studies in site-directed mutants (distances measured from equivalent amino acid Cα atoms of each MDD active site with PyMol[29]). The wild-type funnel area measures ∼145 $Å^2$, whereas the S192A funnel is >2-fold larger at ∼300 $Å^2$. The large S192A funnel size, resulting from the lack of P-loop movement and translation of the β-sheet 9−helix 5 loop away from the active site, accounts for the significantly reduced k_{cat} of S192A MDD. Separately, the D283A funnel is ∼50% smaller than that of the wild type at ∼99 $Å^2$, which is primarily due to novel movements of the β-sheet 9−helix 5 loop. Thus, it seems that the apparently tighter binding of ATP in the D283A mutant can be rationalized by both increased enzyme surface contacts and the more occluded state of the active site funnel that follows nucleotide binding.

DISCUSSION

MDD belongs to a large group of small molecule kinases that is known as the GHMP kinase superfamily.[33] Each of the members in this group catalyzes a sequential reaction, whereby the γ-phosphoryl group of ATP is transferred to an enzyme-specific acceptor, thereby yielding ADP and a phosphorylated product. While a great deal of similarity exists among these

dx.doi.org/10.1021/bi300591x | *Biochemistry* 2012, 51, 5611−5621

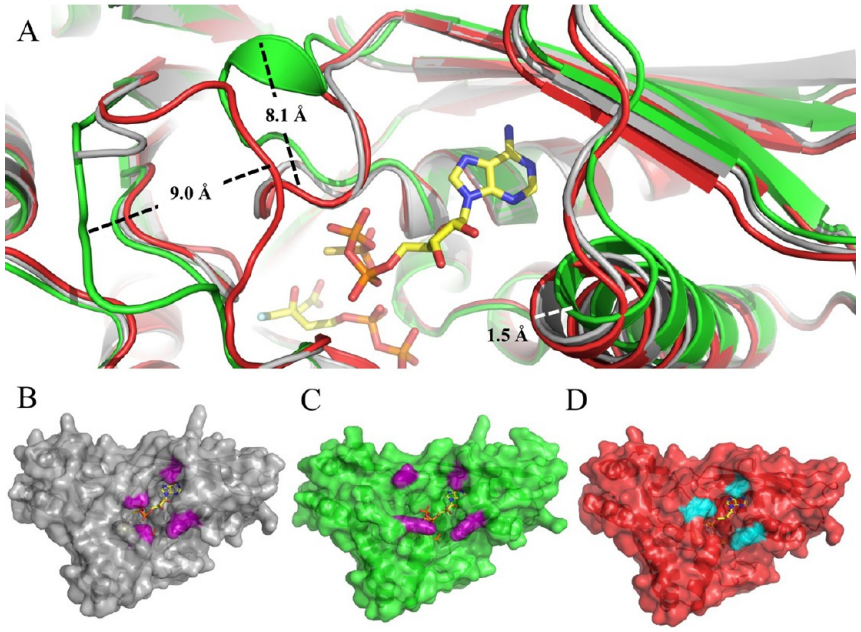

Figure 6. Structural alignment of ternary wild-type and mutant MDD cocrystal structures. (A) Cartoon ribbon diagram of the structural alignment of WT MDD (gray) in complex with the inhibitor FMVAPP and nucleotide analogue ATPγS (balls and sticks, yellow), S192A MDD (green) in complex with the inhibitor FMVAPP and nucleotide analogue ATPγS (not shown for the sake of clarity), and D283A MDD (red) in complex with the substrate MVAPP and nucleotide analogue ATPγS (not shown for the sake of clarity). Measured conformational changes between the S192A and D283A MDD mutants are depicted; distances were measured from equivalent amino acid Cα atoms. (B) Surface representation of the ternary WT MDD cocrystal structure (gray). Area of the active site funnel (~145 Å^2) measured from Ala^{101} Cβ to Lys^{68} Cε (10.5 Å) and Ser^{191} Cα to Leu^{60} CD2 (13.8 Å), with the side chains colored purple. (C) Surface representation of the ternary S192A MDD cocrystal structure (green). Area of the active site funnel (~300 Å^2) measured from Ala^{101} Cβ to Lys^{68} NZ (19.3 Å) and Lys^{188} NZ to Leu^{60} CD2 (15.7 Å), with side chains colored purple. (D) Surface representation of the ternary D283A MDD cocrystal structure (red). Area of the active site funnel (~99 Å^2) measured from Ala^{101} Cβ to Lys^{68} NZ (10.5 Å) and Ser^{187} OG to Leu^{60} CD2 (9.4 Å), with side chains colored cyan.

proteins at the structural level (Cα rmsd values from 2.6 to 4.0 Å),[40] they share relatively low levels of sequence identity (10–20%) overall. This considerable divergence, perhaps reflective of their different acceptor substrates, has given rise to unique combinations of both active site residues and catalytic mechanisms. In addition, the order of substrate binding varies greatly between GHMP kinase family members, with acceptor binding first in some (e.g., mevalonate kinase[39] and MDD [41]), ATP binding first in others (e.g., liver galactokinase,[42] *Salmonella enterica* threonine kinase[43]), and still others incorporating either substrate randomly (e.g., phosphomevalonate kinase[44]). We recently published an article[13] that described the first crystal structures of an MDD bound to two acceptor substrate-like inhibitory analogues. This work demonstrated that the active site of MDD resembles a funnel, with the acceptor substrate binding site and catalytic residues located at the bottom. Given this restriction, it seemed very likely that the MVAPP acceptor binding site would be occluded if the ATP nucleotide donor bound first. The ternary cocrystal structures presented here now demonstrate this point conclusively. In this regard, our structural analyses presented here are consistent with those of Jabalquinto and Cardemil, whose kinetic characterization of avian liver MDD suggested a sequential substrate binding order more than two decades ago.[41]

The binding site of ATPγS within the ternary MDD crystal structure places the γ-phosphoryl ~5.5 Å from the C3-hydroxyl of MVAPP. Such a large distance most likely signifies that this complex has been trapped in a catalytically incompetent state and could have resulted from crystallization with inhibitory mimics of both an acceptor (FMVAPP) and a nucleotide (ATPγS) rather than bona fide substrates. In addition to this, the triphosphoryl group of ATPγS appears to adopt a "kinked" conformation; this may be due to the lack of an ordered Mg^{2+} in any of our ternary cocrystal structures. Nevertheless, a model for a catalytically competent complex can be readily derived by superimposing the AMP-PNP nucleotide analogue found in the *S. pneumoniae* phosphomevalonate kinase ternary complex (PDB entry 3GON) onto the ATPγS nucleotide in the wild-type MDD ternary complex presented here (Figure 7). In this case, the γ-phosphoryl of AMP-PNP is now only 3.4 Å from the C3-hydroxyl of MVAPP and is correctly positioned for in-line phosphoryl transfer.[5] Both mutagenesis[5] and structural studies[13] have implicated Asp^{283} as the catalytic base responsible for deprotonation of the MVAPP C3-hydroxyl. Indeed, the crystal structure of D283A MDD bound to MVAPP (Figure 2B) reveals that mutagenesis of this side chain eliminates the optimal alignment of the C3-hydroxyl of MVAPP. When both the D283A MVAPP and WT MDD ternary complex are considered together (along with previous mutagenesis studies), it appears that the role of Asp^{283} must involve both the deprotonation and optimal orientation of the C3-hydroxyl group of MVAPP.

Considering the structures presented here and elsewhere,[13] along with an array of mutagenesis studies,[5,9,10,13] we can now propose a detailed schematic for the catalytic mechanism of MDD (Figure 8). Asp^{283} correctly positions the MVAPP acceptor substrate, while functioning as a catalytic base to abstract the acidic proton found on its C3-hydroxyl. This deprotonation facilitates an in-line transfer of the γ-phosphoryl from the ATP donor.[5] In addition to the previously discussed catalytic effects of Asp^{283}, several amino acids within the P-loop

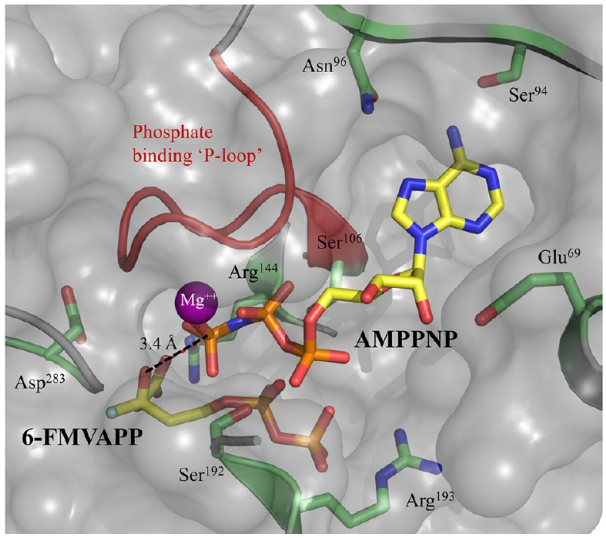

Figure 7. Molecular surface of the substrate and nucleotide binding sites of MDD. An AMP-PNP-Mg^{2+} molecule (yellow, balls and sticks) from phosphomevalonate kinase (PDB entry 3GON) was manually aligned (within COOT[23,24]) on the ATPγS molecule present in the WT MDD ternary cocrystal structure. The surface is rendered semitransparent (gray) with the phosphate binding P-loop (red) and relevant active site side chains (lime) represented as a cartoon ribbon and balls and sticks, respectively. The AMP-PNP γ-phosphoryl is within 3.4 Å of the C3-hydroxyl of FMVAPP (yellow, balls and sticks).

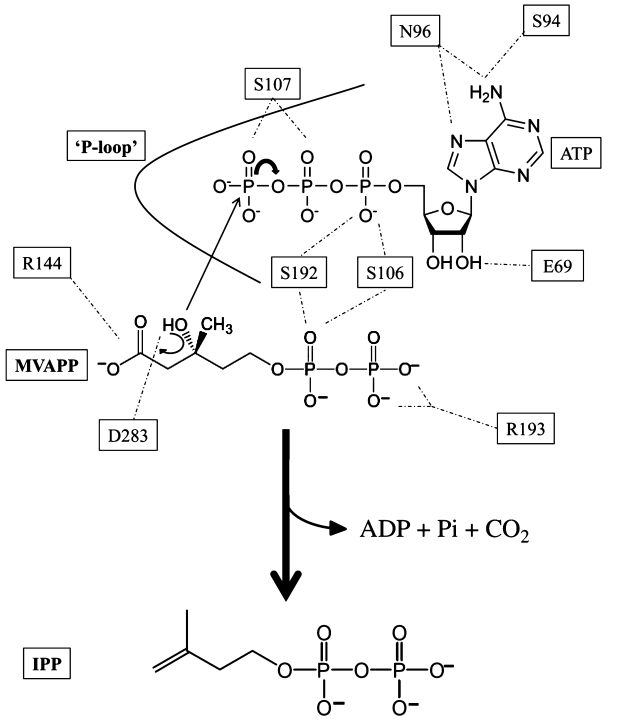

Figure 8. Proposed scheme for the catalytic mechanism of mevalonate diphosphate decarboxylase. Abstraction of the C3-hydroxyl proton from MVAPP is aided by the carboxyl group of Asp^{283}, which functions as the catalytic base in the MDD reaction. Several MDD amino acid side chains within the P-loop interact with the ATP phosphoryl groups. Ser^{107} and Ser^{141} play prominent roles in stabilizing the γ-phosphoryl group. The guanidinium group of Arg^{144} interacts with the MVAPP carboxylate group assisting, in decarboxylation after formation of the carbocation intermediate. Not all ligand interactions within the ternary crystal structure are depicted. Hydrogen bonds are shown as dashed lines.

are involved in extensive interactions with the triphosphoryl group of ATP. These residues are conserved across GHMP kinase family members and include Ala^{105}, Ser^{106}, Ser^{107}, and Ala^{108}. Previous mutagenesis of Ser^{107} [9] revealed only modest changes in the K_d for ATP-Mg and the K_M for MVAPP despite a >42000-fold reduction in k_{cat}. This side chain is appropriately positioned to hydrogen bond with both the β- and γ-phosphoryl groups of ATPγS within the MDD ternary structure, which strongly suggests that its role in MDD catalysis involves properly positioning the ATP phosphoryl groups. Ser^{106} and Ser^{192} each interact with the α-phosphoryl of ATPγS and FMVAPP, which further suggests that their roles involve appropriately aligning both substrate and nucleotide within the active site funnel. Separately, two arginine side chains (Arg^{144} and Arg^{193}) flank either side of the MVAPP acceptor. The guanidinium group of Arg^{144} aids in catalysis by influencing the position of the C1-carboxyl group of MVAPP and promotes decarboxylation. This interaction was disrupted in the D283A ternary complex. Arg^{193}, found only in prokaryotes,[13] interacts with the phosphoryl groups of MVAPP and locks the acceptor in position within the active site. In summary, the reaction mechanism of MDD appears to be quite similar to that of mevalonate kinase[39] and provides further evidence that the GHMP kinases involved in the mevalonate pathway have many features in common with one another.

The human genome encodes more than 500 different kinases, which is perhaps not surprising because phosphoryl transfer events are found in a multitude of biochemical and signal transduction pathways. Because many of these enzymes (e.g., protein kinases in particular) have well-defined roles in serious diseases such as cancer, kinases as a whole have become an extremely popular target of small molecule inhibition studies in recent years.[45] Intriguingly, the development of highly specific small molecule inhibitors has been quite successful despite a high degree of conservation within the respective ATP binding sites of these enzymes.[46] Because it is possible to design truly specific kinase inhibitors for therapeutic use, it seems all the more important that a detailed understanding of both the structure and mechanism of the kinase target be in place prior to beginning this work. Thus, the crystal structures presented within these studies and elsewhere[13] constitute a valuable platform for rational drug design. By employing high-throughput screening with biochemical assays and structure-guided design (through crystallographic data), novel compounds that specifically target mevalonate pathway enzymes may be developed into antimicrobials effective against significant Gram-positive pathogens such as *S. aureus*, *S. epidermidis*, and *E. faecalis*. In this regard, the fact that the mevalonate pathway enzymes have not yet been targeted for antibiotic purposes strongly suggests that any novel inhibitors are likely to be active against deadly bacterial strains already resistant to current therapeutic agents.

■ ASSOCIATED CONTENT

Supporting Information

Four supplemental figures, their corresponding legends, and five supplemental tables. This material is available free of charge via the Internet at http://pubs.acs.org.

dx.doi.org/10.1021/bi300591x | *Biochemistry* 2012, 51, 5611−5621

Accession Codes

The refined coordinates and structure factors (entries 4DPT, 4DPU, 4DPW, 4DPX, 4DPY, 4DU7, and 4DU8) have been deposited in the Protein Data Bank.

AUTHOR INFORMATION

Corresponding Author

*School of Biological Sciences, University of Missouri—Kansas City, 5100 Rockhill Rd., Kansas City, MO 64110. B.V.G.: e-mail, geivnsbrechtB@umkc.edu. H.M.M.: e-mail, miziorkoH@umkc.edu; telephone, (816) 235-2592; fax, (816) 235-1503.

Present Address

§Department of Molecular Biosciences, University of Kansas, 1200 Sunnyside Ave., Lawrence, KS 66045.

Author Contributions

These authors shared supervision of this work.

Funding

This work was supported by National Institutes of Health Grants AI071028 and AI090149 and the Marion-Merrell-Dow Foundation.

Notes

The authors declare no competing financial interest.

ACKNOWLEDGMENTS

We acknowledge the generous technical assistance of SER-CAT staff during X-ray diffraction data collection. Use of the Advanced Photon Source was supported by the U.S. Department of Energy, Office of Science, Office of Basic Energy Sciences, under Contract W-31-109-Eng-38. Data were collected at Southeast Regional Collaborative Access Team (SER-CAT) beamlines at the Advanced Photon Source, Argonne National Laboratory. A list of supporting member institutions may be found at http://www.ser-cat.org/members.html.

ABBREVIATIONS

IPP, isopentenyl diphosphate; MDD, mevalonate diphosphate decarboxylase; DPGP, diphosphoglycolylproline; MVAPP, mevalonate 5-diphosphate; FMVAPP, 6-fluoromevalonate 5-diphosphate; GHMP, galactokinase, homoserine kinase, mevalonate kinase, phosphomevalonate kinase; ATPγS, adenosine 5′-*O*-(thiotriphosphate); AMP-PNP, adenosine 5′-(β,γ-imidotriphosphate); PDB, Protein Data Bank; rmsd, root-mean-square deviation; P-loop, phosphate binding loop.

REFERENCES

(1) Eisenreich, W., Bacher, A., Arigoni, D., and Rohdich, F. (2004) Biosynthesis of isoprenoids via the non-mevalonate pathway. *Cell. Mol. Life Sci. 61*, 1401−1426.

(2) Wilding, E. I., Brown, J. R., Bryant, A. P., Chalker, A. F., Holmes, D. J., Ingraham, K. A., Iordanescu, S., So, C. Y., Rosenberg, M., and Gwynn, M. N. (2000) Identification, evolution, and essentiality of the mevalonate pathway for isopentenyl diphosphate biosynthesis in Gram-positive cocci. *J. Bacteriol. 182*, 4319−4327.

(3) Jabalquinto, A. M., and Cardemil, E. (1987) Kinetic effects of ATP, divalent metal ions and pH on chicken liver mevalonate 5-diphosphate decarboxylase. *Biochim. Biophys. Acta 916*, 172−178.

(4) Bloch, K., Chaykin, S., Phillips, A. H., and De Waard, A. (1959) Mevalonic acid pyrophosphate and isopentenylpyrophosphate. *J. Biol. Chem. 234*, 2595−2604.

(5) Krepkiy, D., and Miziorko, H. M. (2004) Identification of active site residues in mevalonate diphosphate decarboxylase: Implications for a family of phosphotransferases. *Protein Sci. 13*, 1875−1881.

(6) Alvear, M., Jabalquinto, A. M., Eyzaguirre, J., and Cardemil, E. (1982) Purification and characterization of avian liver mevalonate-5-pyrophosphate decarboxylase. *Biochemistry 21*, 4646−4650.

(7) Michihara, A., Sawamura, M., Nara, Y., Ikeda, K., and Yamori, Y. (1997) Purification and characterization of two mevalonate pyrophosphate decarboxylases from rat liver: A novel molecular species of 37 kDa. *J. Biochem. 122*, 647−654.

(8) Chiew, Y. E., O'Sullivan, W. J., and Lee, C. S. (1987) Studies on pig liver mevalonate-5-diphosphate decarboxylase. *Biochim. Biophys. Acta 916*, 271−278.

(9) Krepkiy, D. V., and Miziorko, H. M. (2005) Investigation of the functional contributions of invariant serine residues in yeast mevalonate diphosphate decarboxylase. *Biochemistry 44*, 2671−2677.

(10) Voynova, N. E., Fu, Z., Battaile, K. P., Herdendorf, T. J., Kim, J. J., and Miziorko, H. M. (2008) Human mevalonate diphosphate decarboxylase: Characterization, investigation of the mevalonate diphosphate binding site, and crystal structure. *Arch. Biochem. Biophys. 480*, 58−67.

(11) Bonanno, J. B., Edo, C., Eswar, N., Pieper, U., Romanowski, M. J., Ilyin, V., Gerchman, S. E., Kycia, H., Studier, F. W., Sali, A., and Burley, S. K. (2001) Structural genomics of enzymes involved in sterol/isoprenoid biosynthesis. *Proc. Natl. Acad. Sci. U.S.A. 98*, 12896−12901.

(12) Byres, E., Alphey, M. S., Smith, T. K., and Hunter, W. N. (2007) Crystal structures of *Trypanosoma brucei* and *Staphylococcus aureus* mevalonate diphosphate decarboxylase inform on the determinants of specificity and reactivity. *J. Mol. Biol. 371*, 540−553.

(13) Barta, M. L., Skaff, D. A., McWhorter, W. J., Herdendorf, T. J., Miziorko, H. M., and Geisbrecht, B. V. (2011) Crystal structures of *Staphylococcus epidermidis* mevalonate diphosphate decarboxylase bound to inhibitory analogs reveal new insight into substrate binding and catalysis. *J. Biol. Chem. 286*, 23900−23910.

(14) Zetola, N., Francis, J. S., Nuermberger, E. L., and BIshai, W. R. (2005) Community-acquired meicillin-resistant *Staphylococcus aureus*: An emerging threat. *Lancet Infect. Dis. 5*, 275−286.

(15) Tenover, F. C., Biddle, J. W., and Lancaster, M. V. (2001) Increasing resistance to vancomycin and other glycopeptides in *Staphylococcus aureus*. *Emerging Infect. Dis. 7*, 327−332.

(16) Zhang, J., Yang, P. L., and Gray, N. S. (2009) Targeting cancer with small molecule kinase inhibitors. *Nat. Rev. Cancer 9*, 28−39.

(17) Reardon, J. E., and Abeles, R. H. (1987) Inhibition of cholesterol biosynthesis by fluorinated mevalonate analogues. *Biochemistry 26*, 4717−4722.

(18) Vlattas, I., Dellureficio, J., Ku, E., Bohacek, R., and Zhang, X. (1996) Inhibition of mevalonate 5-pyrophosphate decarbarboxylase by a proline-containing transition state analog. *Bioorg. Med. Chem. Lett. 6*, 2091−2096.

(19) Brøns-Poulsen, J., Nøhr, J., and Larsen, L. (2002) Megaprimer method for polymerase chain reaction-mediated generation of specific mutations in DNA. *Methods Mol. Biol. 182*, 71−76.

(20) Otwinowski, Z., and Minor, W. (1997) Processing of X-ray Diffraction Data Collected in Oscillation Mode. *Methods Enzymol. 276*, 307−326.

(21) McCoy, A., Grosse-Kunstleve, R., Storoni, L., and Read, R. (2005) Likelihood-enhanced fast translation functions. *Acta Crystallogr. D61*, 458−464.

(22) Adams, P. D., Grosse-Kunstleve, R. W., Hung, L. W., Ioerger, T. R., McCoy, A. J., Moriarty, N. W., Read, R. J., Sacchettini, J. C., Sauter, N. K., and Terwilliger, T. C. (2002) PHENIX: Building new software for automated crystallographic structure determination. *Acta Crystallogr. D58*, 1948−1954.

(23) Emsley, P., and Cowtan, K. (2004) Coot: Model-building tools for molecular graphics. *Acta Crystallogr. D60*, 2126−2132.

(24) Emsley, P., Lohkamp, B., Scott, W. G., and Cowtan, K. (2010) Features and development of Coot. *Acta Crystallogr. D66*, 486−501.

(25) Schuttelkopf, A. W., and van Aalten, D. M. (2004) PRODRG: A tool for high-throughput crystallography of protein-ligand complexes. *Acta Crystallogr. D60*, 1355−1363.

(26) Thompson, J., Higgins, D., and Gibson, T. (1994) CLUSTAL W: Improving the sensitivity of progressive multiple sequence alignment through sequence weighting, position-specific gap penalties and weight matrix choice. *Nucleic Acids Res. 22*, 4673−4680.
(27) Gouet, P., Courcelle, E., Stuart, D., and Métoz, F. (1999) ESPript: Analysis of multiple sequence alignments in PostScript. *Bioinformatics 15*, 305−308.
(28) Zemla, A. (2003) LGA: A method for finding 3D similarities in protein structures. *Nucleic Acids Res. 31*, 3370−3374.
(29) DeLano, W. (2002) *The PyMOL Molecular Graphics System*, DeLano Scientific, San Carlos, CA.
(30) Andreassi, J. L., Vetting, M. W., Bilder, P. W., Roderick, S. L., and Leyh, T. S. (2009) Structure of the Ternary Complex of Phosphomevalonate Kinase: The Enzyme and its Family. *Biochemistry 48*, 6461−6468.
(31) Saraste, M., Sibbald, P. R., and Wittinghofer, A. (1990) The P-loop: A common motif in ATP- and GTP-binding proteins. *Trends Biochem. Sci. 15*, 430−434.
(32) Tsay, Y. H., and Robinson, G. W. (1991) Cloning and characterization of ERG8, an essential gene of *Saccharomyces cerevisiae* that encodes phosphomevalonate kinase. *Mol. Cell. Biol. 11*, 620−631.
(33) Bork, P., Sander, C., and Valencia, A. (1993) Convergent evolution of similar enzymatic function on different protein folds: The hexokinase, ribokinase, and galactokinase families of sugar kinases. *Protein Sci. 2*, 31−40.
(34) Mozzarelli, A., and Rossi, G. L. (1996) Protein function in the crystal. *Annu. Rev. Biophys. Biomol. Struct. 25*, 343−365.
(35) Thoden, J. B., Timson, D. J., Reece, R. J., and Holden, H. M. (2005) Molecular structure of human galactokinase: Implications for type II galactosemia. *J. Biol. Chem. 280*, 9662−9670.
(36) Miallau, L., Alphey, M. S., Kemp, L. E., Leonard, G. A., McSweeney, S. M., Hecht, S., Bacher, A., Eisenreich, W., Rohdich, F., and Hunter, W. N. (2003) Biosynthesis of isoprenoids: Crystal structure of 4-diphosphocytidyl-2C-methyl-D-erythritol kinase. *Proc. Natl. Acad. Sci. U.S.A. 100*, 9173−9178.
(37) Zhou, T., Daugherty, M., Grishin, N. V., Osterman, A. L., and Zhang, H. (2000) Structure and mechanism of homoserine kinase: Prototype for the GHMP kinase superfamily. *Structure 8*, 1247−1257.
(38) Krishna, S. S., Zhou, T., Daugherty, M., Osterman, A., and Zhang, H. (2001) Structural basis for the catalysis and substrate specificity of homoserine kinase. *Biochemistry 40*, 10810−10818.
(39) Fu, Z., Wang, M., Potter, D., Miziorko, H. M., and Kim, J. J. (2002) The structure of a binary complex between a mammalian mevalonate kinase and ATP: Insights into the reaction mechanism and human inherited disease. *J. Biol. Chem. 277*, 18134−18142.
(40) Andreassi, J. L., and Leyh, T. S. (2004) Molecular functions of conserved aspects of the GHMP kinase family. *Biochemistry 43*, 14594−14601.
(41) Jabalquinto, A. M., and Cardemil, E. (1989) Substrate binding order in mevalonate 5-diphosphate decarboxylase from chicken liver. *Biochim. Biophys. Acta 996*, 257−259.
(42) Ballard, F. J. (1966) Purification and properties of galactokinase from pig liver. *Biochem. J. 98*, 347−352.
(43) Fan, C., Fromm, H. J., and Bobik, T. A. (2009) Kinetic and Functional Analysis of L-Threonine Kinase, the PduX Enzyme of *Salmonella enterica*. *J. Biol. Chem. 284*, 20240−20248.
(44) Pilloff, D., Dabovic, K., Romanowski, M. J., Bonanno, J. B., Doherty, M., Burley, S. K., and Leyh, T. S. (2003) The kinetic mechanism of phosphomevalonate kinase. *J. Biol. Chem. 278*, 4510−4515.
(45) Cohen, P. (2002) Protein kinases: The major drug targets of the twenty-first century? *Nat. Rev. Drug Discovery 1*, 309−315.
(46) Davies, S. P., Reddy, H., Caivano, M., and Cohen, P. (2000) Specificity and mechanism of action of some commonly used protein kinase inhibitors. *Biochem. J. 351*, 95−105.